Nuclear Engineering and Technology 55 (2023) 295–303

Contents lists available at ScienceDirect

Nuclear Engineering and Technology

journal homepage: www.elsevier.com/locate/net

Original Article

Determination of counting efficiency considering the biodistribution of ^{131}I activity in the whole-body counting measurement

MinSeok Park [a, c, *], Jaeryong Yoo [a], Minho Kim [b], Won Il Jang [a], Sunhoo Park [a]

[a] National Radiation Emergency Center, Korea Institute of Radiological and Medical Sciences, Seoul, 01812, Republic of Korea
[b] Department of RI Application, Korea Institute of Radiological and Medical Sciences, Seoul, 01812, Republic of Korea
[c] Department of Nuclear Engineering, Hanyang University, Seoul, 04763, Republic of Korea

ARTICLE INFO

Article history:
Received 28 April 2022
Received in revised form
18 August 2022
Accepted 12 September 2022
Available online 18 September 2022

Keywords:
Whole-body counter
Monte Carlo simulation
Computational phantom
Counting efficiency
Radioiodine

ABSTRACT

Whole-body counters are widely used to assess internal contamination after a nuclear accident. However, it is difficult to determine radioiodine activity due to limitations in conventional calibration phantoms. Inhaled or ingested radioiodine is heterogeneously distributed in the human body, necessitating time-dependent biodistribution for the assessment of the internal contamination caused by the radioiodine intake. This study aims at calculating counting efficiencies considering the biodistribution of ^{131}I in whole-body counting measurement. Monte Carlo simulations with computational human phantoms were performed to calculate the whole-body counting efficiency for a realistic radioiodine distribution after its intake. The biodistributions of ^{131}I for different age groups were computed based on biokinetic models and applied to age- and gender-specific computational phantoms to estimate counting efficiency. After calculating the whole-body counting efficiencies, the efficiency correction factors were derived as the ratio of the counting efficiencies obtained by considering a heterogeneous biodistribution of ^{131}I over time to those obtained using the BOMAB phantom assuming a homogeneous distribution. Based on the correction factors, the internal contamination caused by ^{131}I can be assessed using whole-body counters. These correction factors can minimize the influence of the biodistribution of ^{131}I in whole-body counting measurement and improve the accuracy of internal dose assessment.

1. Introduction

After a nuclear accident, population monitoring should be performed to assess the radiation doses to the potentially exposed population [1]. Radiation instruments are required for population monitoring, and in such cases, whole-body counters (WBCs) are generally used to assess internal contamination in the affected population. In the case of the Fukushima nuclear accident, large-scale population monitoring using WBCs was conducted for residents, including the evacuees living in the Fukushima prefecture to estimate the internal dose [2,3].

The calibration of a WBC is required to guarantee accurate activity estimates. The bottle manikin absorption (BOMAB) phantom, which consists of a cylindrical-shaped plastic container with a radioactive solution of known activity, is used as a calibration standard for WBCs to simulate a homogeneously contaminated individual [4]. Notwithstanding the usefulness of the BOMAB phantom in the calibration of WBCs, it has limitations associated with differences in anatomy, attenuation properties, and activity distribution between the physical phantom and human body [5–8]. Inhaled or ingested radionuclides are heterogeneously distributed in the human body due to their biological movement. This can influence the accuracy of whole-body counting, in particular the counting efficiency [8,9]. The distribution of radioactivity in the human body can vary with the intake scenarios, including the radionuclide, pathway, and elapsed time after the intake, as incorporated radionuclides tend to accumulate in specific organs after entering through the respiratory or gastrointestinal tract [9]. In experimental calibration, the BOMAB phantom does not simulate the heterogeneous distribution of radionuclides based on their biokinetic models, which can significantly influence whole-body counting [7]. Furthermore, the accuracy of whole-body counting measurements is dependent on the anatomical discrepancies between the physical calibration phantom and the individual under assessment [10,11]. The physical characteristics of the individual

* Corresponding author. National Radiation Emergency Center, Korea Institute of Radiological and Medical Sciences, Seoul, 01812, Republic of Korea.
E-mail address: chulipak@kirams.re.kr (M. Park).

https://doi.org/10.1016/j.net.2022.09.013

being assessed in population monitoring may differ according to body-build, age, and gender [2,12]. BOMAB phantoms can be prepared in different sizes for WBC calibration, however, this would be non-practical and costly in terms of managing radioactive substances [13]. Thus, it is necessary to use alternative methods to study the influence individual anatomy and radionuclide biodistribution on the counting efficiency of WBCs.

Virtual calibration, based on Monte Carlo simulation with a computational human phantom, has been suggested to address the limitations of conventional WBC calibration [5,14,15]. By increasing the computing power, the virtual calibration can be conveniently employed in the calculation of counting efficiencies in WBCs. Anatomical realism can be achieved using advanced computational phantoms. Furthermore, the biodistribution, depending on the different intake scenarios, can be simulated with the Monte Carlo code, using the virtual calibration method [9]. From an internal dose assessment perspective, the accuracy of measurements can be improved using computational phantoms in the calibration of WBCs.

Whole-body counting measurements have a higher sensitivity compared to those of other *in vivo* measurements, which leads to limitations in the assessment of internal contamination by radionuclides heterogeneously distributed in the body. To improve the accuracy of internal contamination assessment for these radionuclides in the whole-body counting measurement, it is necessary to consider the time-dependent biodistribution after its intake, particular, radioiodine. The radioiodine that is released during nuclear accidents primarily accumulates in the thyroid gland following intake and is heterogeneously distributed in the body [16]. It is difficult to measure the retained radioiodine using WBCs because a homogeneous distribution of radioiodine in the whole-body of an individual is assumed [17]. Therefore, this study aims at estimating the counting efficiencies considering the time-dependent biodistribution of ^{131}I in whole-body counting measurements. Based on the biokinetic model, the activity distribution of ^{131}I in the human body was calculated and simulated using computational phantoms. The individuals inhaling or ingesting radionuclides following an accident are of different ages and genders. Thus, the counting efficiency for various ages and genders were calculated using age- and gender-specific computational phantoms. The relationship between the counting efficiencies estimated considering a time-dependent biodistribution and those estimated considering a homogeneous distribution was determined; this was done to calculate the efficiency correction factors in the whole-body counting measurement for population monitoring.

2. Materials and methods

Two types of commercial WBCs currently in operation at the Korea Institute of Radiological and Medical Sciences were modeled using a Monte Carlo N-Particle (MCNP) transport code, version 6.2 [18], developed by Los Alamos National Laboratory. Fig. 1 shows the representations of both systems, based on the manufacturer's documents and the implemented computational geometries. One is a stand-up type WBC system (FASTSCAN; Canberra Industries, Meriden, CT, USA), consisting of two NaI(Tl) with the crystal dimensions of 7.6 cm × 12.7 cm × 40.6 cm. The other is a bed type WBC system (ACCUSCAN; Canberra Industries, Meriden, CT, USA), consisting of two high-purity germanium (HPGe) radiation detectors with crystal dimensions of 6.2 cm (diameter) × 4.1 cm (length) and 6.2 cm (diameter) × 3.6 cm (length). Both WBCs use linear counting geometry, which can minimize the dependence of the counting efficiency on the size of the individual being measured [19,20]. The stand-up type WBC does not involve any moving parts during the measurement. However, the bed type WBC is a horizontal scanning counter with a moving bed and it automatically moves along the length of the individual. It is necessary to modify the measurement geometry, in particular the scanning bed, when performing Monte Carlo simulations because MCNP code cannot simulate the moving geometry directly. Thus, the simulation geometry of the bed type WBC was modified to represent the movement of the scanning bed as a sum of individual steps, based on the previous study [21]. As a result (Fig. 1b), the counting efficiency could be simultaneously calculated using 12 separate positions of radiation detectors while optimizing the computational time and geometric movement of the WBC.

In Monte Carlo simulations, the counting efficiencies for each photo-peak in the spectra were calculated by employing the pulse height tally (F8 tally) with the Gaussian energy broadening (GEB) function available in the MCNP code. F8 tally was applied to the virtual detectors in both WBCs, which scored the pulses created in the detector volume per photon emitted from the source in a given energy bin. The energy bins of the pulse-height spectra were determined corresponding to the number of energy channels in the WBC systems (stand-up type WBC: 512 channels and bed type WBC: 8192 channels). The GEB function was used to simulate the energy resolution of NaI(Tl) and HPGe crystals in detection systems based on the full-width at half maximum obtained via the energy calibration of the WBC. The computationally modeled geometries of both WBCs have been validated by comparing the counting efficiencies obtained from the simulation with those obtained from the experimental calibration. Based on the validated simulation geometries of stand-up and bed type WBCs, the Monte Carlo simulations were performed to calculate the counting efficiency. The number of simulated particles (2.5×10^8) was selected in such a way that the statistical uncertainties in the F8 tally results were below 5% in all simulations.

Computational phantoms were used to represent the individuals contaminated by inhaling or ingesting radionuclides following an accident. The counting efficiencies for the whole-body counting measurements was simulated using the age- and gender-specific computational phantoms. Unlike the conventional calibration phantom for WBCs, these computational phantoms can represent realistic anatomical characteristics and the heterogeneous distribution of the internal organs, including tissues, and skeletal components. The adult reference computational phantoms published by the International Commission on Radiological Protection (ICRP) [22] and the reference hybrid family phantoms (5, 10, and 15 years in age) released by the University of Florida/National Cancer Institute (UF/NCI) [23] were used in the present study. A brief overview of the computational phantoms used in this study is summarized in Table 1.

One-year-old computational phantoms were not considered in this study due to the potential risk of injury and reduction in accuracy while performing whole-body counting with small children. In the case of the Fukushima accident, the whole-body counting measurements were performed for individuals aged 4 years or older [17,24]. BABYSCAN, along with other types of WBCs were suggested to measure the internal contamination for children below the age of 4-year-old [25].

The computational phantoms were placed in the equivalent position of an adult male BOMAB phantom to maintain the reproducibility of the measurement geometry. However, the sensitivity of a stand-up type WBC is decreased for children, mainly because of their height. This is primarily because the sensitivity is designed for the measurement of the working population, including the adult male and female [19]. For practical whole-body counting measurements of children, lifting tools were implemented to prevent the reductions in the counting efficiency of the stand-up type WBC.

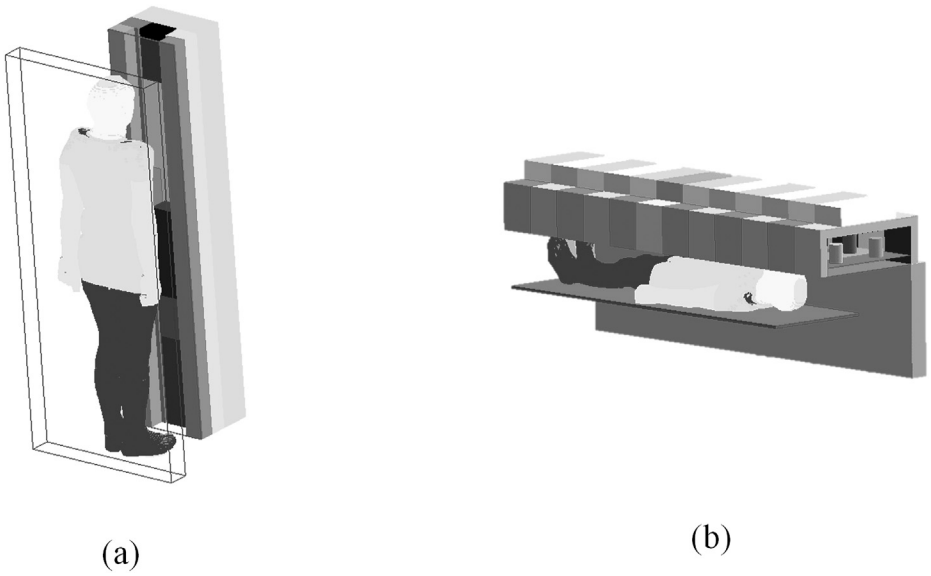

Fig. 1. Simulation geometry for whole-body counting measurement: (a) stand-up type WBC, (b) bed type WBC.

Table 1
The anatomical information of the male and female computational phantoms.

Phantom	Gender	Height (cm)	Weight (kg)	Voxel dimensions (mm)
UF/NCI 5 y	male	109	18	0.85 × 0.85 × 1.928
	female	109	18	
UF/NCI 10 y	male	138	32	0.99 × 0.99 × 2.425
	female	138	32	
UF/NCI 15 y	male	167	57	1.25 × 1.25 × 2.832
	female	161	53	1.20 × 1.20 × 2.828
ICRP reference adult	male	176	73	2.137 × 2.137 × 8.00
	female	163	60	1.775 × 1.775 × 4.84

Thus, the position of 5- and 10-year-old computational phantoms in the stand-up type WBC were elevated, based on the ratio between the heights of the ICRP adult male and female reference computational phantoms and the placement of the lower side detector (distance of 61 cm above the bottom), to improve the sensitivity of whole-body counting measurement. These position modifications were dependent on the gender of the computational phantoms. The simulation geometries for the 5- and 10-year-old computational phantoms in the stand-up type WBC are shown in Fig. 2.

The distribution of radioactivity in the body is assumed to be homogeneous in typical whole-body counting. However, the biodistribution of radionuclide can differ depending on various internal contamination scenarios [8]. It can also vary with the age and gender of the individual being assessed [9]. The biodistribution of radionuclide, inhaled or ingested, is an important parameter in analyzing the internal contamination in individuals, as the counting efficiency of *in-vivo* measurements can be affected by the distribution of radioactivity retained in the body. This study aimed to investigate the time-dependent biodistributions of ^{131}I at five

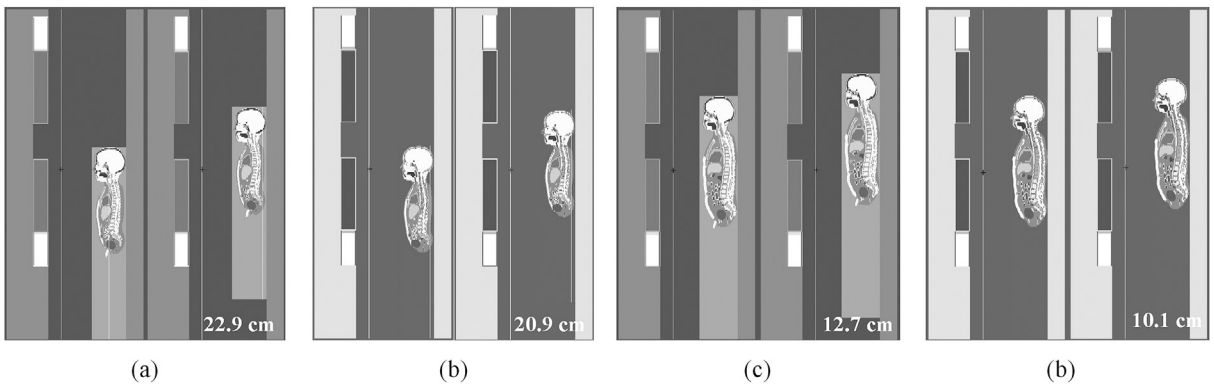

Fig. 2. The simulation geometry in the stand-up type WBC for the 5- and 10-year computational phantoms: (a) 5-year-old male, (b) 5-year-old female, (c) 10-year-old male, (d) 10-year-old female.

stages of human development (5 y, 10 y, 15 y, and adult), corresponding to different internal contamination scenarios, and subsequently calculate the whole-body counting efficiency. The amount of ^{131}I retained in an organ after a specific time was estimated using the Dose and Risk Calculation (DCAL) software (version 9.4), provided by the Center for Biokinetics and Dosimetry Research at the Oak Ridge National Laboratory [26]. The activities of radioiodine over time in various anatomical regions for individuals of different age groups after the incorporation of 1 Bq were calculated using the ACTACAL module of the DCAL software.

To calculate the time-dependent whole-body counting efficiency for population monitoring, the intake scenarios based on the environmental exposure pathways were considered. The inhalation and ingestion of ^{131}I, which were the main contributors of internal contamination in the previous nuclear power plant accident, were considered as the intake pathways. Several parameters, including the activity median aerodynamic diameter (AMAD), absorption type, and absorption fraction (f_1), have to be determined, in order to calculate the fraction of radioactivity present in each body compartment after intake. In the present study, these parameters were determined based on the recommended default values for environmental exposure. The absorption of inhaled ^{131}I was considered as type F, the recommended absorption type for assessing public exposure [27]. For intake by inhalation, radioiodine was considered to have 1 μm of AMAD, as recommended for internal dose assessment in environmental exposures [28,29].

Based on age-specific biokinetic models and parameters that depend on the intake scenario, the activity distributions of ^{131}I in the body were calculated for each age group. An elapsed time range of 1–90 days following the intake was considered, based on the population monitoring in the Fukushima nuclear accident. In the case of the Fukushima nuclear accident, the whole-body counting measurement was performed within approximately three months to assess the affected population in the vicinity of the accident [1,30]. This time interval was used to calculate the time-dependent biodistributions in body compartments following the acute intake of radionuclide. The distribution of ^{131}I, calculated using the DCAL software, was applied to the computational phantoms to estimate the counting efficiency. The source particles generated in the Monte Carlo simulations can be distributed in the organs or tissues depicted by the computational phantoms, to represent the internally contaminated individuals. However, there is a problem related to the application of biodistributions to computational phantoms. The DCAL software provides the amount of radioactivity in compartments based on biokinetic models. These compartments do not completely correspond to anatomical regions in the computational phantoms. Some organs are not fully segmented in computational phantoms due to limitations in voxel resolutions. To accurately simulate the activity distribution in the computational phantoms, it was necessary to establish relationships between the anatomical regions of adult and pediatric computational phantoms and the compartments of biokinetic models used in the DCAL software. A blood region is not completely represented in computational phantoms due to limited voxel resolution. Notably, the mass of blood represented in each computational phantom is significantly less than the reference value of blood mass [31]. Thus, the radioactivity in the blood compartment was assumed to be homogeneously distributed over the body tissues [7]. Furthermore, the alveolar-interstitial (AI), bronchiolar (bb), and bronchial (BB) regions are the compartments of the respiratory tract in the biokinetic model. The activity fraction of each region is estimated using the DCAL software. However, the AI, bb, and BB regions are not fully segmented in the computational phantoms, as the sizes of these regions are excessively small to be represented in a voxel geometry. The activity fractions of the AI, bb, and BB regions are folded into the lung and bronchial tree and thus represented in computational phantoms. The amount of activity fraction in each compartment of biokinetic models was distributed into the structures of computational phantoms corresponding to the mass proportions of each anatomical regions [9].

3. Results and discussion

Before acquiring the whole-body counting efficiency, the validation of the computational modeling geometries of both WBCs was conducted based on a comparison of the counting efficiencies for the simulation and experimental calibration. The simulations were benchmarked using the adult male BOMAB phantom to calculate the counting efficiency of the WBCs. Fig. 3 shows a comparison of the counting efficiencies that are obtained from the simulation and measurement in both WBC systems; it showed a similar trend for all photo-peak energies of the calibration source. The averaged relative deviations between the simulated and measured counting efficiencies were 4.5% and 4.6% for stand-up and bed type WBCs, respectively. Thus, the counting efficiencies obtained from the simulation were in good agreement with those obtained from the measurement. Based on these validation results,

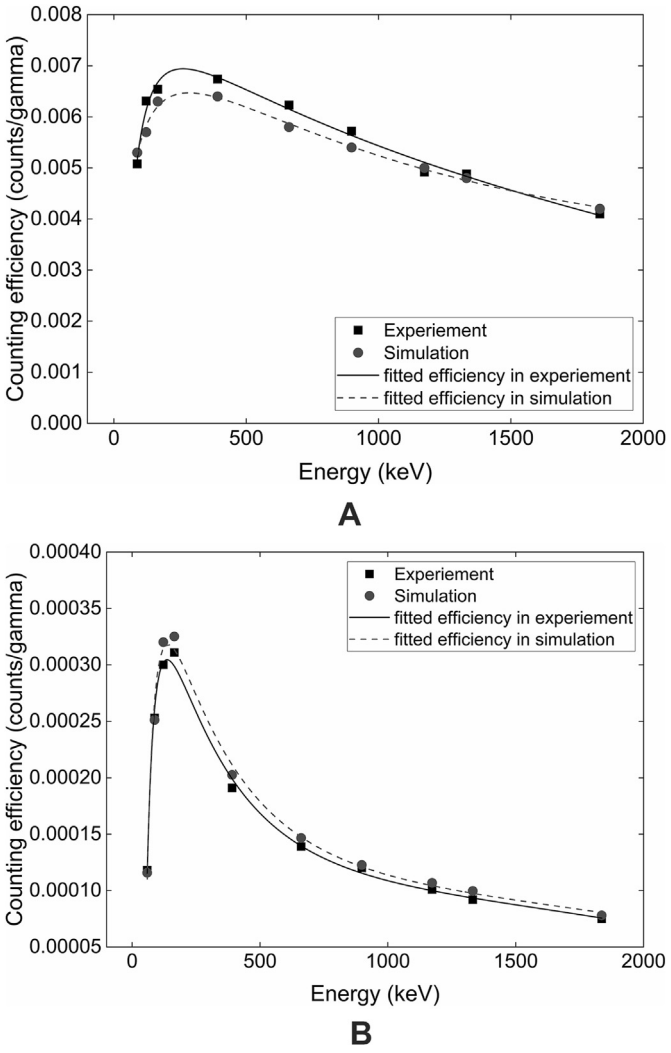

Fig. 3. Counting efficiencies obtained from the simulation and experimental calibration for an adult male BOMAB phantom as a function of gamma radiation energy: (a) stand-up type WBC, (b) bed type WBC.

the computational modeling geometries of both WBCs were applied to computational phantoms to calculate the whole-body counting efficiencies in given conditions.

The time-dependent counting efficiencies for the 364 keV photo-peak of ^{131}I were obtained using the age- and gender- specific computational phantoms, considering the distribution of the radionuclide activity over time. The counting efficiencies considering the biodistribution of ^{131}I were compared with those considering a homogeneous distribution to investigate the influence of the distribution of ^{131}I activity in whole-body counting. The efficiency correction factors were calculated as the ratio between the counting efficiencies obtained from the computational phantoms, considering the biodistribution of ^{131}I and those obtained from the BOMAB phantom. Figs. 4 and 5 show the efficiency correction factors for both WBCs as a function of elapsed time after the intake in the considered exposure scenario of ^{131}I inhalation. In the case of stand-up type WBC (Fig. 4), the efficiency correction factors rapidly decrease during the first few days following the intake and then gradually become constant at approximately 10, 20, 30, and 60 days for a 5-year-old, 10-year-old, 15-year-old, and an adult, respectively. The tendency of efficiency correction factors depending on the elapsed time after the intake is similar to that in the bed type WBC (Fig. 5), where the efficiency correction factors become constant at approximately 6, 8, 20, and 35 days for a 5-year-old, 10-year-old, 15-year-old, and an adult, respectively, after the intake of ^{131}I.

The efficiency correction factors as a function of elapsed time after the intake of ^{131}I ingestion are shown in Figs. 6 and 7 for the stand-up and bed type WBCs, respectively. In contrast to inhalation exposure, the efficiency correction factors for all age groups sharply increase in the first few days following the intake, due to the biological movement of ingested ^{131}I. The influence of the biodistribution of ^{131}I on the counting efficiency is considerably dominant in the case of ^{131}I ingestion. Efficiency correction factors for both WBC systems increase in the first 3 days after the intake and then decreased to constant values of correction factors. The efficiency correction factors for the stand-up type WBC are 1.7, 1.72, 2.23, 2.15, 2.34, 2.43, 2.16, and 2.21 for 5-year-old male, 5-year-old female, 10-year-old male, 10-year-old female, 15-year-old male, 15-year-old female, an adult male, and an adult female, respectively. In the bed type WBC, the efficiency correction factors for each age group are equal to 1.61, 1.70, 1.65, 1.49, and 1.46 for a 5-year-old, 10-year-old, 15-year-old, an adult male, and an adult female, respectively.

The efficiency correction factors for stand-up type WBC show different tendencies compared to those for bed type WBC. In the case of inhaled ^{131}I, the efficiency correction factors for the stand-up and bed type WBCs are within the ranges of 1.7–3.0 and 1.5–2.3, respectively. The ranges of efficiency correction factors for the stand-up and bed type WBCs for ^{131}I ingestion are 1.6–2.5 and 1.4–1.7, respectively, across all age groups studied. This is mainly because of the difference in measurement geometries for both WBCs. A bed type WBC uniformly scans the whole-body of individual. However, the detectors for a stand-up type WBC are placed facing the adult torso in measurement. The efficiency correction factors of the bed type WBC are smaller than those of the stand-up type WBC, which implies that the geometry of the bed type WBC is less influenced by the biodistribution of radioiodine than that of the stand-up type WBC.

The differences in whole-body counting efficiencies as a function of elapsed time after the intake are caused by the activity distribution of radioiodine. Figs. 8 and 9 represent the activity fraction of inhaled and ingested ^{131}I retained in anatomical regions by age group after intake, respectively. The retention of ^{131}I in the human body, calculated using the DCAL software, represents the amount of radioiodine accumulated in the body tissues (muscle, adipose tissue) and internal organs (including thyroid, blood vessels, and large intestine). Based on these biological movements of ^{131}I, the inhaled or ingested radioiodine is heterogeneously distributed within the human body as a function of time.

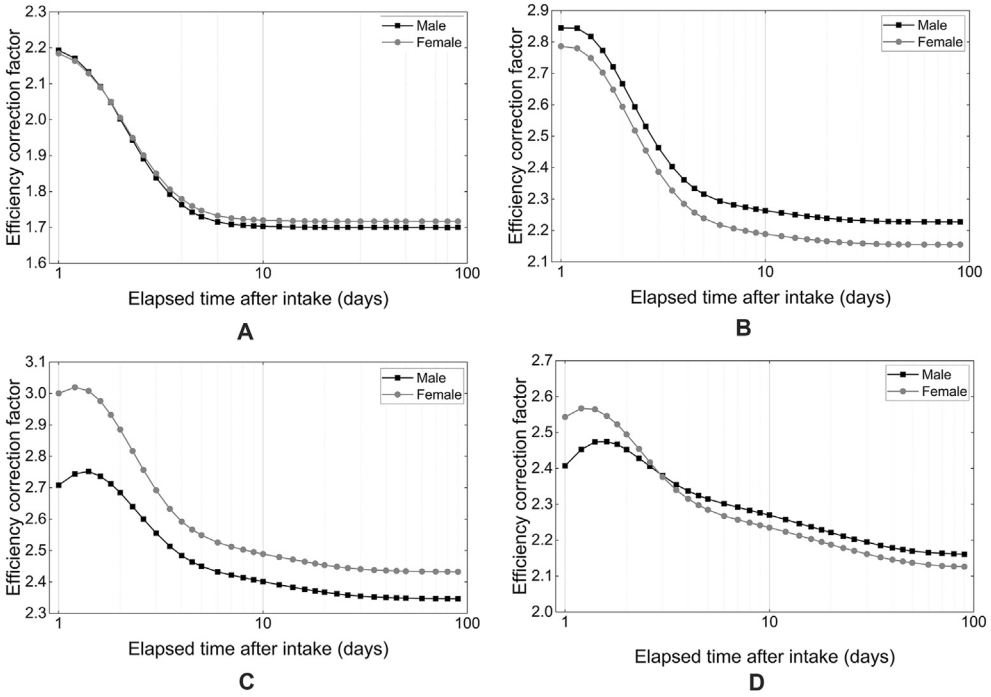

Fig. 4. Efficiency correction factors as a function of elapsed time after the intake of ^{131}I inhalation in the stand-up type WBC: (a) 5-year-old, (b) 10-year-old, (c) 15-year-old, (d) adult.

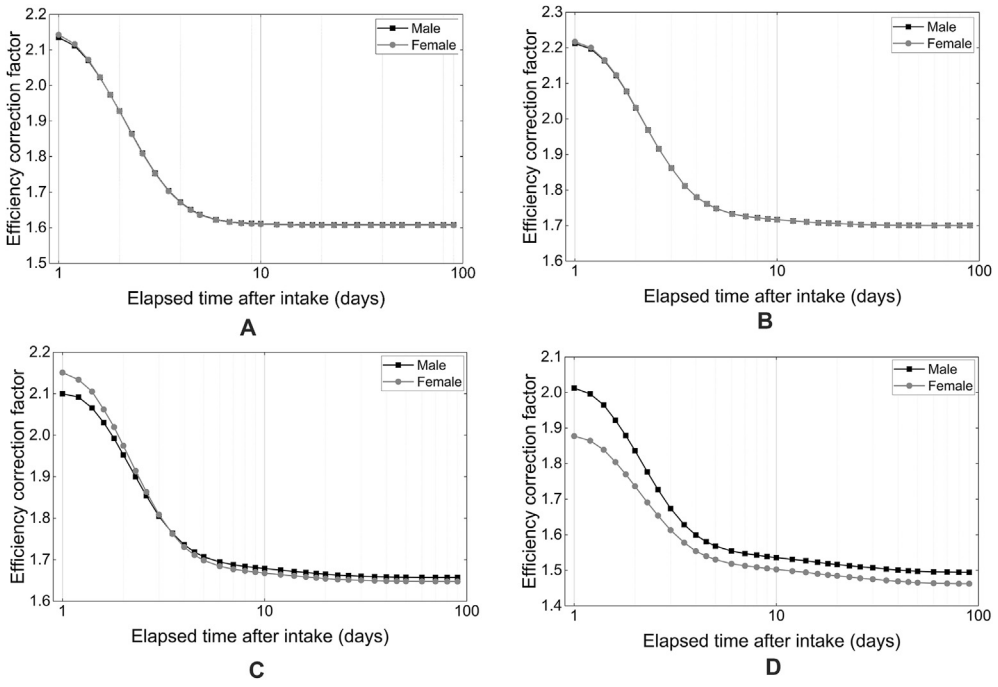

Fig. 5. Efficiency correction factors as a function of elapsed time after the intake of ^{131}I inhalation in the bed type WBC: (a) 5-year-old, (b) 10-year-old, (c) 15-year-old, (d) adult.

As represented in Fig. 8, the inhaled ^{131}I mainly accumulates in the thyroid and is also distributed in body tissue and some internal organs including the extrathoracic region and blood vessels. In particular, the retained ^{131}I in the extrathoracic region dramatically decreased but that in the body tissue gradually increased in the initial phase (approximately 10 days) after the incorporation. These biological movements of inhaled ^{131}I causes the variation of counting efficiencies for both WBCs. The efficiency correction factors become constant after the initial phase because most of the ^{131}I is distributed in the thyroid and body tissue. The tendency of efficiency correction factors differs according to the age group, although there is no clear difference in biokinetic model calculations for ^{131}I for different age group. These differences of efficiency correction factors are caused by the anatomical differences between the age groups. In particular, the size of internal organs and body tissues differ according to the age group of the measured individuals, which could further affect the whole-body counting efficiency. The activity distribution of ingested ^{131}I in different

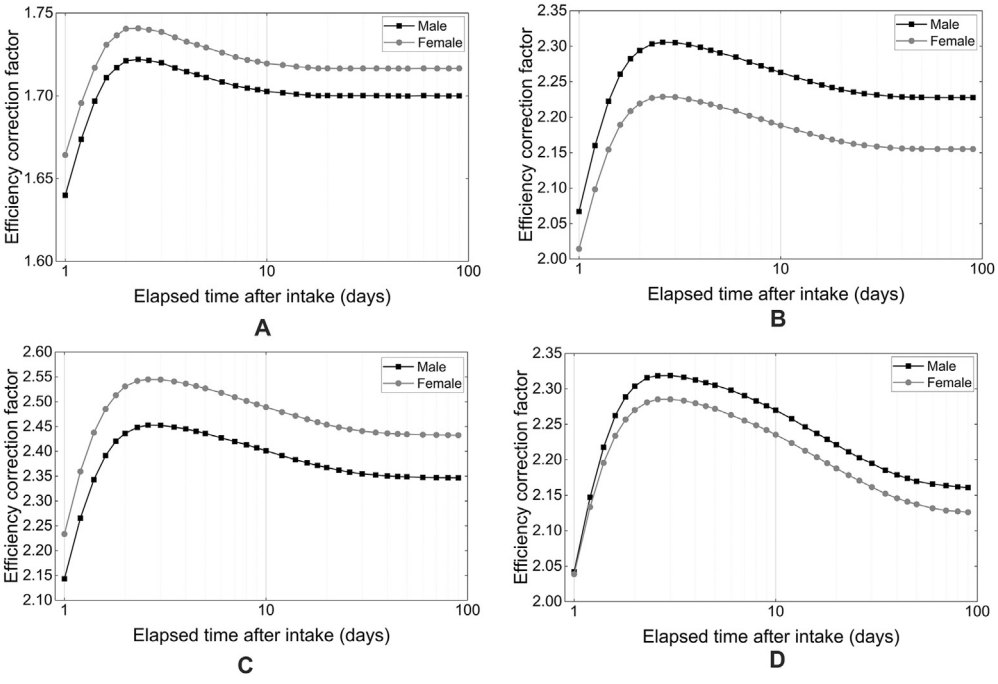

Fig. 6. Efficiency correction factors as a function of elapsed time after the intake of ^{131}I ingestion in the stand-up type WBC: (a) 5-year-old, (b) 10-year-old, (c) 15-year-old, (d) adult.

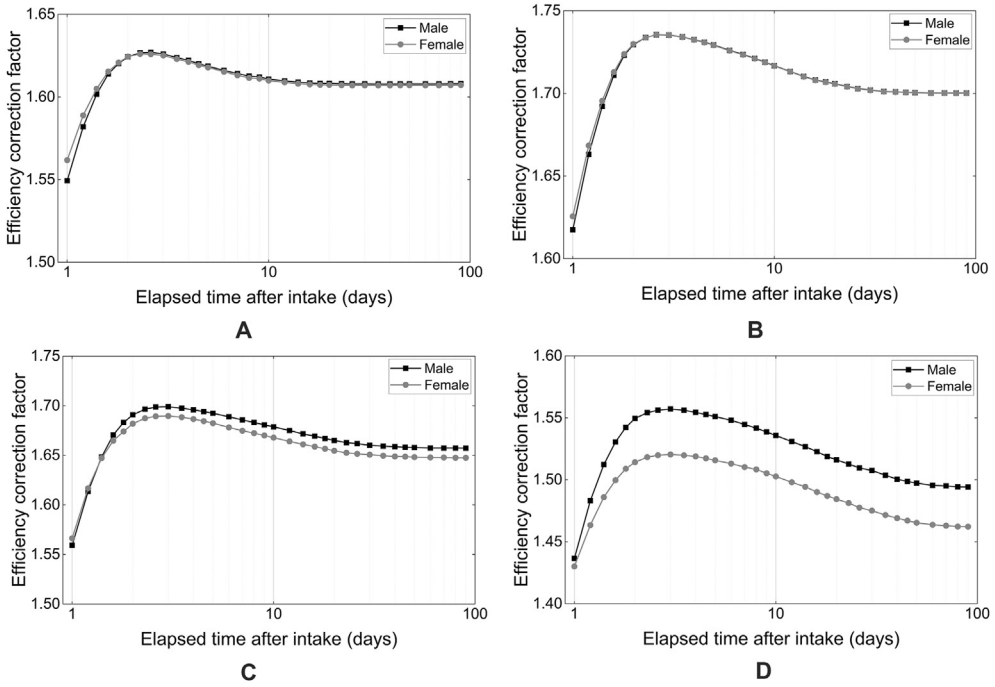

Fig. 7. Efficiency correction factors as a function of elapsed time after the intake of ^{131}I ingestion in the bed type WBC: (a) 5-year-old, (b) 10-year-old, (c) 15-year-old, (d) adult.

anatomical regions after intake is shown in Fig. 9. Similar to the inhalation case, the ingested ^{131}I was mainly distributed in the thyroid, body tissue, and blood vessels. However, there was no anatomical region that represented the rapid decrement of activity fraction as time elapsed after intake. The activity fractions in blood vessels, the large intestine, and the urinary bladder decreased but that in body tissue gradually increased in the initial phase after intake. Because of the biodistribution of ^{131}I after intake, the tendency of efficiency correction factors in the ingestion case is different from that in the inhalation case.

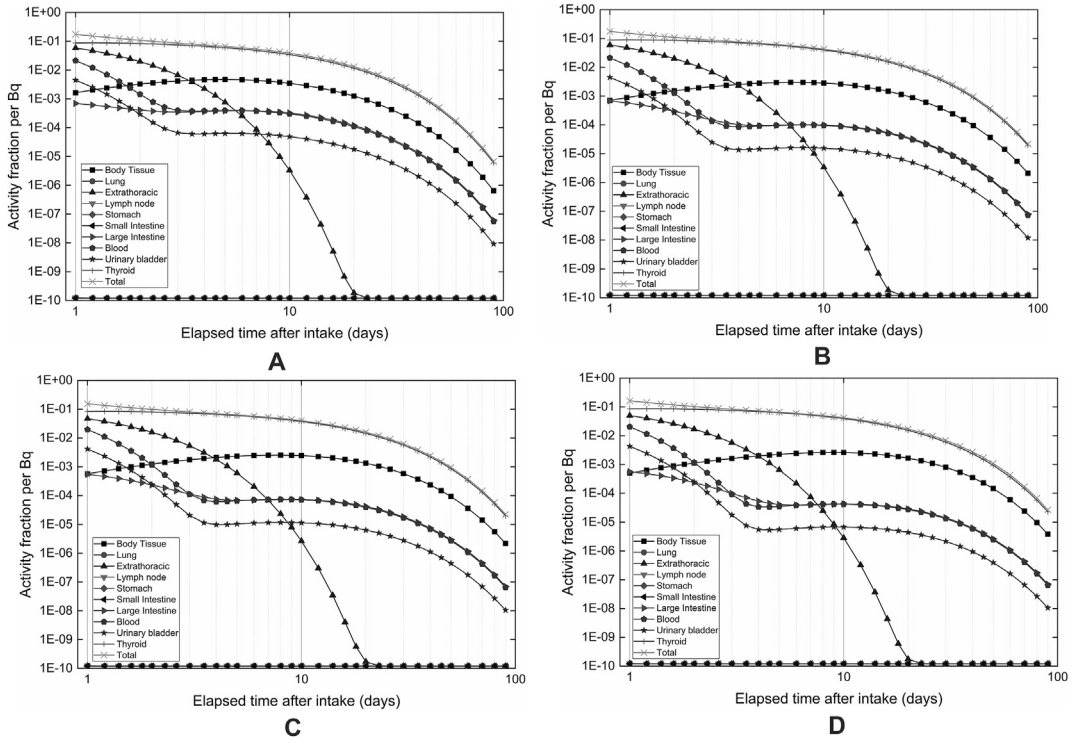

Fig. 8. Activity fraction of inhaled ^{131}I per Bq retained in the anatomical regions as a function of elapsed time after intake: (a) 5-year-old, (b) 10-year-old, (c) 15-year-old, (d) adult.

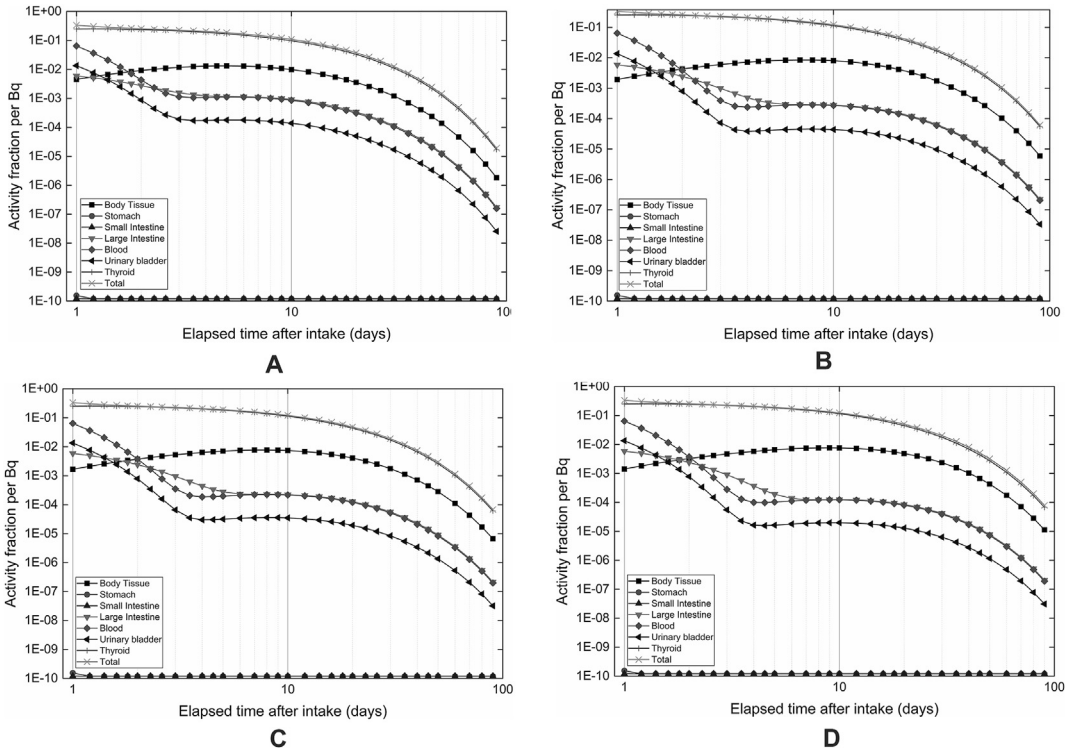

Fig. 9. Activity fraction of ingested ^{131}I per Bq retained in the anatomical regions as a function of elapsed time after intake: (a) 5-year-old, (b) 10-year-old, (c) 15-year-old, (d) adult.

The results demonstrate that the biodistribution of ^{131}I significantly influences the counting efficiency for both WBCs used in this study. The counting efficiencies, considering the distribution of ^{131}I activity, are double the values obtained from the BOMAB phantom considering the homogeneous distribution. If the counting efficiency calculated using the BOMAB phantom was applied in the whole-body counting measurement, the internal contamination of ^{131}I could be substantially overestimated compared to the actual contamination in the individual. Therefore, it is necessary to apply efficiency correction factors for minimizing the influence of the biodistribution of ^{131}I in whole-body counting measurement. The whole-body counting efficiency considering the biodistribution of ^{131}I can be derived by applying the efficiency correction factors to the counting efficiency obtained with the BOMAB phantom assuming a homogeneous activity distribution.

4. Conclusions

This study performed virtual calibration to calculate counting efficiencies in accordance with the biodistribution of ^{131}I in two commercial WBCs. The whole-body counting measurement has a limitation associated with measuring the individuals internally contaminated by radioiodine after a nuclear emergency owing to the influence of biodistribution on the counting efficiency. To address this issue, the efficiency correction factors were derived from the ratios of the counting efficiencies considering the biodistribution of ^{131}I to those considering a homogeneous distribution, obtained with the conventional BOMAB phantom. The efficiency correction factors were provided for different age groups to consider the anatomical characteristics depending on the age and gender of measured individuals. The results showed that the ^{131}I activity estimates that were measured using a WBC can be overestimated by more than double in the absence of correction factors, which can lead to an incorrect assessment of internal exposure for a population. Therefore, we believe that the age- and gender-specific efficiency correction factors calculated using the virtual calibration method can provide an accurate activity estimate of ^{131}I in the whole-body counting measurement for population monitoring.

These results suggest that the heterogeneous activity distribution of retained radionuclide has significant impact on the whole-body counting efficiency. The intake scenarios were concerning in terms of the acute intake to calculate the biodistribution of radioiodine. However, internal contamination can occur through various intake scenarios, including the chronic intake of radioiodine following an accident. Thus, in future research, it is necessary to investigate the whole-body counting efficiency considering various intake scenarios to reduce the error in activity estimates caused by the influence of biodistribution.

Declaration of competing interest

The authors declare that they have no known competing financial interests or personal relationships that could have appeared to influence the work reported in this paper.

Acknowledgments

This study was supported by a grant of the Korea Institute of Radiological and Medical Sciences (KIRAMS), funded by Ministry of Science and ICT(MSIT), Republic of Korea (No.50535–2022) and the Nuclear Safety Research Program through the Korea Foundation Of Nuclear Safety (KoFONS) using the financial resource granted by the Nuclear Safety and Security Commission (NSSC) of Republic of Korea (No. 2104038). The authors thank Choonsik Lee of the National Cancer Institute for providing valuable data on computational phantoms.

References

[1] O. Kurihara, E. Kim, K. Tani, M. Ogawa, K. Yajima, M. Kowatari, H. Tatsuzaki, Effective population monitoring for determination of the thyroidal radioiodine content of the public following a nuclear accident in Japan, Environmental Advances 8 (2022), 100206.

[2] O. Kurihara, C. Li, M.A. Lopez, E. Kim, K. Tani, T. Nakano, C. Takada, T. Momose, M. Akashi, Experiences of population monitoring using whole-body counters in response to the Fukushima nuclear accident, Health Phys. 115 (2) (2018) 259–274.

[3] E. Kim, O. Kurihara, N. Kunishima, T. Nakano, K. Tani, M. Hachiya, T. Momose, T. Ishikawa, S. Tokonami, M. Hosoda, M. Akashi, Early intake of radiocesium by residents living near the TEPCO Fukushima Dai-ichi nuclear power plant after the accident. Part 1: internal doses based on whole-body measurements by NIRS, Health Phys. 111 (5) (2016) 451–464.

[4] Health Physics Society, American National Standard: specifications for the bottle manikin absorption phantom, ANSI/HPS N13 (1999) 35.

[5] M. Park, H.S. Kim, J. Yoo, C.H. Kim, W.I. Jang, S. Park, Virtual calibration of whole-body counters to consider the size dependency of counting efficiency using Monte Carlo simulations, Nucl. Eng. Technol. 53 (2) (2021) 4122–4129.

[6] B. Zhang, M. Mille, X.G. Xu, An analysis of dependency of counting efficiency on worker anatomy for in vivo measurements: whole-body counting, Phys. Med. Biol. 53 (13) (2008) 3463–3475.

[7] J. Bento, S. Barros, P. Teles, P. Vaz, M. Zankl, Efficiency correction factors of an ACCUSCAN whole-body counter due to the biodistribution of ^{134}Cs, ^{137}Cs and ^{60}Co, Radiat. Protect. Dosim. 155 (1) (2013) 16–24.

[8] W.E. Bolch, J.L. Hurtado, C. Lee, R. Manager, E. Burgett, N. Hertel, W. Dickerson, Guidance on the use of handheld survey meters for radiological triage: time-dependent detector count rates corresponding to 50, 250, and 500 mSv effective dose for adult male and females, Health Phys. 102 (3) (2012) 305–325.

[9] R. Anigstein, R.H. Olsher, D.A. Loomis, A. Ansary, Use of transportable radiation detection instruments to assess internal contamination from intakes of radionuclides Part II: calibration factors and ICAT computer program, Health Phys. 111 (6) (2016) 542–558.

[10] E. Carinou, V. Koukouliou, M. Budayova, C. Potiriadis, V. Kamenopoulou, The calculation of a size correction factor for a whole-body counter, Nucl. Instrum. Methods Phys. Res. 580 (1) (2007) 197–200.

[11] D. Krstic, O. Cuknic, D. Nikezic, Application of MCNP5 software for efficiency calculation of a whole body counter, Health Phys. 102 (6) (2012) 657–663.

[12] D. Krstic, D. Nikezic, Efficiency of whole-body counter for various body size calculated by MCNP5 software, Radiat. Protect. Dosim. 152 (2012) 179–183.

[13] M. Park, J. Yoo, W.H. Ha, S. Park, Y.W. Jin, Measurement and simulation of the counting efficiency of a whole-body counter using a BOMAB phantom inserted with rod sources containing mixed radionuclides, Health Phys. 114 (3) (2018) 282–287.

[14] Y. Chen, R. Qiu, C. Li, Z. Wu, J. Li, Construction of Chinese adult male phantom library and its application in the virtual calibration of in vivo measurement, Phys. Med. Biol. 61 (5) (2016) 2124–2144.

[15] T.C.F. Fonseca, A.L. Lebacq, L.C. Mihailescu, F. Vanhavere, R. Bogaerts, Development of a 3D human body library based on polygonal mesh surface for whole body counter set-up calibration, Prog.Nucl. Sci. Technol. 4 (2014) 614–618.

[16] S. Nagataki, Thyroid consequences of the Fukushima nuclear reactor accident, Eur Thyroid J 1 (2012) 148–159.

[17] K. Tani, Y. Igarashi, E. Kim, T. Iimoto, O. Kurihara, Monte-Carlo simulations with mathematical phantoms to investigate the effectiveness of a whole-body counter for thyroid measurement, Radiat. Meas. 135 (2020).

[18] C.J. Werner, MCNP User's Manual Code Version 6.2, Los Alamos National Laboratory, 2017. LA-UR-17-29981.

[19] F.L. Bronson, L.F. Booth, D.D. Richards, Fastscan – a computerized, anthropometrically designed, high throughput, whole body counter for the nuclear industry, in: Proceedings of the Seventeenth Midyear Topical Symposium of the Health Physics Society, 1984. Pasco, USA, https://mirion.s3.amazonaws.com/cms4_mirion/files/pdf/technical-papers/fastscan.pdf?1534969742. also available at.

[20] F.L. Bronson, The ACCUSCAN-II vertical scanning germanium whole body counter, in: Proceedings of the International Congress of the International Radiation Protection Association (IRPA), 1988. Sydney, Australia, https://mirion.s3.amazonaws.com/cms4_mirion/files/pdf/technical-papers/accuscan.pdf?1534969731. also available at.

[21] G.H. Kramer, L.C. Burns, S. Guerriere, Monte Carlo simulation of a scanning detector whole body counter and the effect of BOMAB phantom size on the calibration, Health Phys. 83 (4) (2002) 526–533.

[22] ICRP 110, Adult reference computational phantoms, in: Pergamon Press Publication 110, Ann, vol. 49, ICRP, Oxford, 2009, 3.

[23] ICRP 143, Paediatric reference computational phantoms, in: Pergamon Press Publication 143, Ann, vol. 49, ICRP, Oxford, 2020, 1.

[24] T. Momose, C. Takada, T. Nakagawa, K. Kanai, O. Kurihara, N. Tsujimura, Y. Ohi, T. Murayama, T. Suzuki, Y. Uezu, S. Furuta, Whole-body counting of Fukushima residents after the TEPCO Fukushima Daiichi nuclear power station accident, in: Proceedings of the First NIRS Symposium on the Reconstruction of Early Internal Dose in the TEPCO Fukushima Daiichi Nuclear Power Station Accident, National Institute of Radiological Sciences; NIRS-M-252, Chiba, Japan, 2012, pp. 67–82.

[25] R.S. Hayano, Sh Yamanaka, F.L. Bronson, B. Oginni, I. Muramatsu, BABSCAN: a whole-body counter for small children in Fukushima, J. Radiol. Prot. 34 (2014) 645–653.

[26] K.F. Eckerman, R.W. Leggett, M. Cristy, C.B. Nelson, J.C. Ryman, A.L. Sjoreen, R.C. Ward, Dose and Risk Calculation Software, 2006. Oak Ridge: ORNL/TM-2001/190).

[27] ICRP 119, Compendium of dose coefficients based on ICRP publication 60, ICRP publication 119 ICRP41 (Suppl.) (2012). Ann.

[28] ICRP 72, Age-dependent doses to the members of the public from intake of radionuclides. Part 5: compilation of ingestion and inhalation coefficients, ICRP Publication 72, Ann. ICRP 26 (1) (1995).

[29] ICRP 66, Human respiratory tract model for radiological protection, ICRP publication 66, Ann. ICRP 24 (1–3) (1994).

[30] T. Ishikawa, Radiation doses and associated risk from the Fukushima nuclear accident: a review of recent publications, Asia Pac. J. Publ. Health 29 (2S) (2017) 18S–28S.

[31] ICRP 145, Adult mesh-type reference computational phantoms, ICRP publication 145, Ann. ICRP49(3), 2020.